SCIENCE CHINA
Earth Sciences

• RESEARCH PAPER •

doi: 10.1007/s11430-012-4405-4

Numerical study on the response of the Earth's magnetosphere-ionosphere system to a super solar storm

WANG Chi[1*], LI Hui[1,2], GUO XiaoCheng[1], DING Kai[1,2] & HUANG ZhaoHui[1]

[1] *State Key Laboratory of Space Weather, Center for Space Science and Applied Research, Chinese Academy of Sciences, Beijing 100190, China;*
[2] *Graduate School of Chinese Academy of Sciences, Beijing 100049, China*

Received March 3, 2011; accepted February 15, 2012

With the approaching of the 24th solar cycle peak year (2012–2014), the impacts of super solar storms on the geospace environment have drawn attentions. Based on the geomagnetic field observations during Carrington event in 1859, we estimate the interplanetary solar wind conditions at that time, and investigate the response of the magnetosphere-ionosphere system to this extreme solar wind conditions using global 3D MHD simulations. The main findings include: 1) The day-side magnetopause and bow shock are compressed to 4.3 and 6.0 Re (Earth radius), and their flanks are also strongly compressed. The magnetopause shifts inside the geosynchronous orbit, exposing geosynchronous satellites in the solar wind in the magnetosheath. 2) During the storm, the region-1 current increases by about 60 times, and the cross polar potential drop increases by about 80 times; the reconnection voltage is about 5 to 6 times larger than the average storms, which means a larger amount of the solar wind energy enters the magnetosphere, resulting in strong space weather phenomena.

space weather, solar storm, magnetosphere-ionosphere system, numerical simulation

Citation: Wang C, Li H, Guo X C, et al. Numerical study on the response of the Earth's magnetosphere-ionosphere system to a super solar storm. Sci China Earth Sci, 2012, doi: 10.1007/s11430-012-4405-4

Solar activity can result in extreme changes of the Earth's space environment, and thereby affect the spaceborne and ground-based high-technology systems of aerospace, communication, navigation, positioning, and electric power system. With the approaching of the 24th solar cycle peak year (2012–2014), the impacts of super solar storms on the geospace environment are getting more concerned. Historically, the first recorded solar flare occurred on September 1, 1859. Two British astronomers witnessed and recorded a series of progresses caused by that solar flare, and Lord R. C. Carrington was one of them. In fact, the white light flare observed by Carrington was only a part of the series of large-scale solar activities and terrestrial effects. This solar flare and subsequent extreme geospace disturbances are called the "Carrington Event", which was the first and strongest space weather event caused by violent solar activities, and was linked to a series of terrestrial responses. During the event of this superstorm, the *Dst* index declined to below −1500 nT, and strong aurora also appeared unusually in the low latitudes. The *Dst* index is derived by averaging the hourly values of the horizontal components of the magnetic field variation from four ground stations evenly distributed in different longitudes near the magnetic equator. Usually, the *Dst* index for a magnetic storm is greater than −200 nT. The Carrington event seriously affected the telegraph services at that time. A significant portion of the world's 200000 km of telegraph lines was adversely affected, many of which were unusable for eight hours or longer,

*Corresponding author (email: cw@spaceweather.ac.cn)

which had a great economic impact [1–3]. However, humans did not enter the space era in 1859, and their dependence on space was not as much as today's society. If a storm similar to the Carrington Event occurred in the modern society, Odenwald et al. [4] estimated that the potential economic loss was about $70 billion.

The earth's magnetosphere-ionosphere system is an important component of the geospace environment. The position and shape of the bow shock and magnetopause are always the most concerned issues of the large-scale structures in the magnetosphere. Based on the satellite observations, empirical formulas about the bow shock and magnetopause were proposed [5, 6]. All the empirical formulas were obtained by statistically analyzing crossing events of the bow shock and magnetopause by satellites. However, such events were very rare under the conditions of intense magnetic storms. So the descriptions of the bow shock and magnetopause under the conditions of intense magnetic storms are basically not of statistical significance. Shue et al. [7] gave the position and shape of the magnetopause as a function of solar wind dynamic pressure (P_d) and southward component (B_Z) of the interplanetary magnetic field (IMF). Owing to the lack of events with IMF $B_Z < -20$ nT, Shue et al. [7] could not give a reasonable fitting curve from the data. When IMF $B_Z < -20$ nT, Shue's empirical model would even fail. The IMF B_Z during the Carrington Event was estimated to be under −60 nT. As a result, the relevant empirical formulas of the position and shape of the bow shock and magnetopause were not applicable any longer. On the other hand, due to the restrictions of satellite orbits, crossing events of the bow shock and magnetopause were concentrated in the day-side low-latitude regions. The observations of the bow shock and magnetopause were rare in the high latitudes. Except for magnetospheric large-scale structures, the large-scale current systems in the magnetosphere-ionosphere system play an important role in affecting the magnetic field in geospace environment, which has distinct properties under extreme interplanetary conditions. For example, under normal interplanetary conditions (with solar wind bulk speed of about 400 km/s, and IMF B_Z of about −5 nT), the region-1 field-aligned current (FAC) is closed through the magnetopause current, and the magnetopause can be regarded as a "dynamo" of the region-1 FAC. However, recent numerical simulations show that the region-1 FAC increases, while the magnetopause current decreases under the conditions of magnetic storm with a strong southward IMF B_Z. At that time, the bow shock contributes to the region-1 FAC, and provides a channel for the solar wind to impact the ionosphere directly [8]. Therefore, using the numerical simulation to analyze the earth's magnetosphere-ionosphere system under extreme interplanetary conditions is the most effective research approach. Ridley et al. [9] studied the responses of the magnetosphere and ionosphere to an extreme large interplanetary shock and coronal mass ejection (CME) event similar to the Carrington Event, by using the global 3D MHD model (BATSRUS) [10] developed by the University of Michigan. Their main concerns were the propagation and interaction progresses of the disturbances in the magnetosphere-ionosphere system. They did not quantitatively describe the changes of near- earth space environment key parameters, such as the magnetospheric large-scale structure, region-1 FAC, cross polar potential drop, and so on. In this work, we will start with geomagnetic observations of the Carrington Event in 1859, estimate the interplanetary conditions, and study the responses of the earth's magnetosphere-ionosphere system to the extreme intense solar storm by analyzing the simulations of our global 3D MHD model. Quantitative variations of the earth's large-scale structures, region-1 FAC and cross polar potential drop in the ionosphere would also be presented to improve our quantitative understanding of the consequences of extreme adverse space weather events.

1 Estimating the interplanetary conditions of the Carrington Event

Satellites were not available when the Carrington Event occurred, therefore there were no interplanetary solar wind data available. But the geomagnetic observations on the ground had a very long history. Based on the ground geomagnetic observations, we can estimate the interplanetary conditions under some theoretical assumptions.

According to the magnetometer records for the 1–2 September 1859 Carrington Event at Colaba Observatory in Mumbai, India, the *Dst* index first increased to its peak value of about 120 nT, and then depressed to under −1500 nT [11]. By using an updated *Dst* prediction model from Li et al. [12], Temerin and Li [13] reproduced the evolution of the *Dst* index of the Carrington Event quite well. In their calculation, the solar wind density was 40 cm^{-3} after the arrival of the shock, and then it sharply increased to 1800 cm^{-3}; the solar wind bulk speed quickly increased to 1200 km/s from 450 km/s first, and then slowly increased to 1750 km/s; during that period, the southward IMF B_Z reached to −68 nT. Based on the ground magnetic observations, Wang et al. [14] estimated the change of the square root of solar wind dynamic pressure across an interplanetary shock. Their statistical analysis showed that there was a good correlation between interplanetary shocks and variations of the *Dst* index. The empirical formula of the amplitudes of sudden impulses (ΔSYM-H) and the change of square root of solar wind dynamic pressure (ΔP_d) was summarized as $\Delta\sqrt{P_d} = 0.056 \times \Delta\,\mathrm{SYM}\text{–}H(\mathrm{nPa}^{1/2})$. The change of square root of solar wind dynamic pressure for the Carrington Event was estimated to be 6.7 $\mathrm{nPa}^{1/2}$, similar to the result calculated from the solar wind parameters estimated by Li

et al. [12]. Taking the above estimations as a reference, we select the following solar wind parameters to mimic the interplanetary conditions of the Carrington Event, as shown in Figure 1: (1) Initial solar wind conditions. B_Z = 2 nT, N = 5 cm^{-3}, V_X = −450 km/s, T = 0.91 × 10^5 K. (2) Storm-time solar wind conditions. B_Z = −60 nT, N = 40 cm^{-3}, V_X = −1500 km/s, T = 14 × 10^5 K.

2 Numerical simulations

Using our self-developed global 3D PPMLR-MHD model [15], we investigate the responses of the earth's magnetosphere-ionosphere system to the above super solar storm, focusing on the changes of geospace environment parameters, such as the large-scale structures, region-1 FAC, and cross polar potential drop in the ionosphere.

The numerical scheme adopted by PPMLR-MHD model is of three-order spatial precision and two-order temporal precision, with a very small numerical dissipation. A shock or a discontinuity front can be captured within two grids. We take a Cartesian coordinate system with the origin at the Earth's center and the x axis pointing to the Sun. The simulation box extends from 30 R_E to −300 R_E in the x direction and from 0 R_E to 150 R_E in the y and z directions. The Earth's magnetosphere-ionosphere system is assumed to be symmetrical to the noon-midnight meridian and equatorial planes. The whole domain is discretized into 160 × 80 × 80 grids: a uniform mesh is laid out in the near-Earth domain of $-10 \leqslant x \leqslant 10$ R_E, $0 \leqslant y, z \leqslant 10$ R_E, with 0.4 R_E in spacing; the grid spacing outside increases according to a geometrical series of common ratio 1.05 along each axis. The inner boundary is set to be at r = 3 R_E, and the electrostatic model is adopted to consider the coupling of the inner boundary and ionosphere. For simplicity, a uniform conductivity model for the ionosphere is used in this case, and the Pedersen and Hall conductances are of 15 S and 0 S, respectively. The interplanetary conditions can be adjusted through the front inflow boundary at x = 30 R_E, while free outflow conditions are applied for the outflow boundary at x = −300 R_E. The calculation process is divided into two steps: first, we fix the initial solar wind conditions, and let the calculation continue until a quasi-static magnetosphere-ionosphere system is reached; at the second step, we introduce the storm-time solar wind conditions shown in Figure 1 into the inflow boundary at x = 30 R_E.

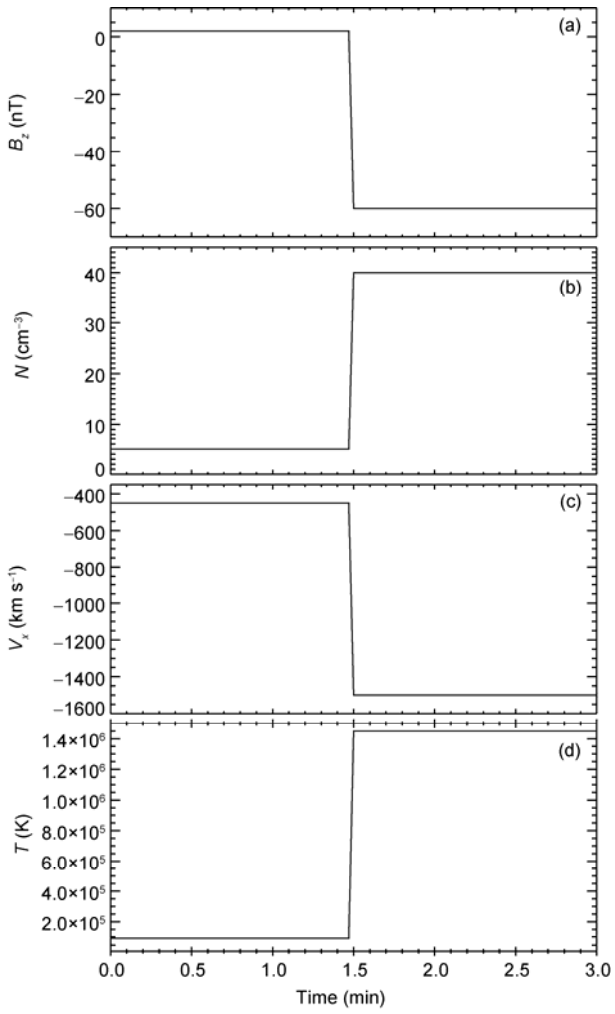

Figure 1 Estimations of the interplanetary conditions for the Carrington Event. (a) The IMF B_Z, (b) solar wind number density, (c) solar wind bulk speed, (d) tempreature.

Figure 2 shows the magnetospheric large-scale structures in the noon-midnight meridian plane obtained from our simulation. The colors represent the distribution of the x component of plasma speed (V_X). Figure 2(a) shows the typical magnetosphere structure under the background solar wind conditions before the arrival of the super solar storm. The yellow circle represents the Earth, the dash dot circle in red represents the geosynchronous orbit, and the dashed and dotted lines in red represent the fitting curves of the magnetopause and bow shock, respectively. The magnetopause and bow shock cut the x axis at 8.5 and 12.0 R_E, respectively, which are in agreement with the results calculated from Shue-98 empirical formula [7].

Figure 2(b) shows the corresponding magnetospheric large-scale structures at about four minutes after introducing the interplanetary conditions of the super solar storm. Due to the rapid enhancement of the solar wind dynamic pressure and southward turning of IMF B_Z, the magnetopause is strongly compressed. At the same time, the geomagnetic field at the dayside magnetopause is also extremely eroded. The magnetopause and bow shock along the x axis are at 4.3 and 6.0 R_E, respectively, implying that the dayside magnetopause and bow shock shift earthward of the geosynchronous orbit (about 6.6 R_E from the center of the Earth). Based on the statistical analysis of 211 magnetic storms, Li et al. [16] found that the 360° panoramic views of geosynchronous B_Z signature for storms of different intensities

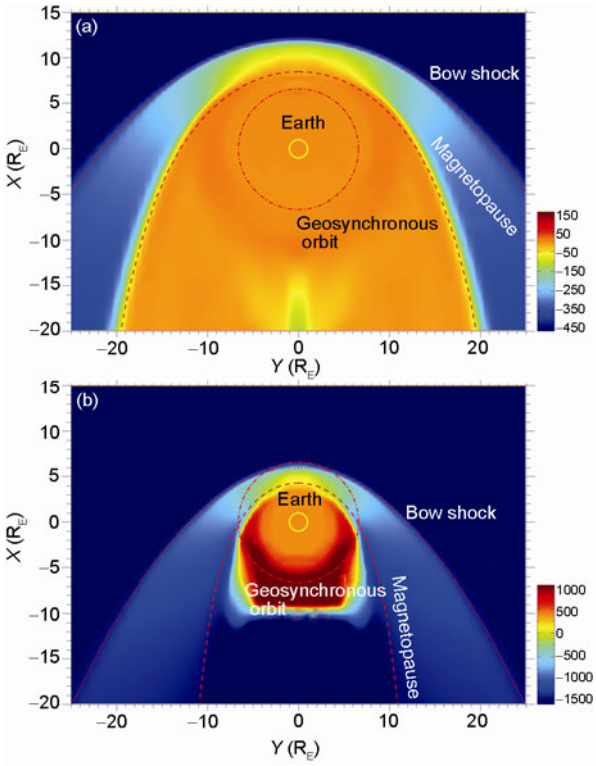

Figure 2 Magnetospheric large-scale structures in the noon-midnight meridian plane (contour plot of the x component of plasma speed, V_X). (a) Under the typical interplanetary conditions; (b) about four minutes after the arrival of the super solar storm.

differ significantly from each other. For small to moderate storms ($-100 < Dst \leqslant -50$ nT), the distribution of B_Z is similar to a bell-shaped Gaussian distribution, peaking on the noon side and reducing to the night side. For the superstorms ($Dst \leqslant -300$ nT), the Gaussian-like distribution even reverses, mainly because the dayside magnetopause is compressed and eroded inside the geosynchronous orbit during super solar storms. During a very intense magnetic storm, the dayside magnetopause commonly shifts earthward of the geosynchronous orbit. The geostationary orbit satellites are therefore directly exposed to the solar wind, and thus more vulnerable to the sun cosmic ray due to the lack of the magnetosphere's protection. Meanwhile, the franks of the bow shock and magnetopause are also compressed strongly. The intersections of the bow shock and y, z axis both reduce from 21.5 R_E to about 12 R_E. The intersections of the magnetopause and y, z axis reduce from 13.0 R_E and 13.5 R_E to 6.5 R_E and 7.7 R_E, respectively. As for the compressions of the franks, the estimations from Shue-98 empirical formula do not match those from the simulations. For example, the magnetopause cuts the y axis at 9.1 R_E from the empirical formula, which is much larger than that of 6.5 R_E from the simulation. Owing to the lack of the samples under very intense magnetic storms, the position and shape of the magnetopause under extreme solar wind conditions from empirical formula cannot fully reflect the real situations.

The strong compression effect of the super solar storm will cause a rapid enhancement of the magnetopause current to balance the extreme solar wind pressure. This will also cause a great increase of the ionospheric current and a series of aurora activities. When the situation gets worse, the aurora activities would even extend to the low latitudes [17]. In this simulation, the peak current density of the region-1 FAC is 0.15 μA/m^2, and the amount is 0.22 MA before the extreme solar wind conditions. After the arrival of the super solar storm, the region-1 FAC increases rapidly, with the peak current density and amount reaching 7.43 μA/m^2 and 13.08 MA, respectively, about 60 times larger than the previous values. Meanwhile, the aurora extends to the low latitudes. Because of the extreme southward IMF B_Z and high-speed solar wind, the region-1 FAC increases rapidly, while the enhancement of the magnetopause current cannot provide sufficient support. At this time, the bow-shock current closes with the region-1 FAC, and becomes a "power source" of the region-1 FAC. It is estimated that more than 50 percentage of region-1 FAC comes from the bow shock. Under extreme solar wind conditions, the solar wind-magnetosphere-ionosphere system can directly input the electromagnetic energy into the ionosphere through this current system.

Magnetic reconnection is a major approach of the solar wind-magnetosphere coupling. The reconnection rate can be quantitatively described by the tangential electric field along the reconnection line, and equals the total potential drop along the reconnection line (reconnection voltage). In the view of ideal MHD, the magnetic field line can be regarded as equipotential; therefore, the cross polar potential drop in the ionosphere equals the reconnection voltage, and thus be directly used to measure the reconnection rate by some researchers [18]. In this case, the cross polar potential drop in the ionosphere has increased by more than 80 times, from 10.6 to 868.2 kV. The Joule heating has also increased by more than 480 times. Siscoe et al. [19] made some extensions about Hill model of the transpolar potential [20, 21], obtaining the relationship of the cross polar potential drop on the solar wind parameters and the Pedersen conductance in the ionosphere. They pointed out that the saturation level of the cross polar potential drop was positively correlated with the solar wind dynamic pressure, whereas it was negatively correlated with the Pedersen conductance in the ionosphere. Assuming the Pedersen conductance to be 15 S during this superstorm, we estimate the cross polar potential drop to be 860.8 kV under the solar wind conditions mentioned in section 1, which is consistent with our numerical simulation. The Carrington Event was accompanied by a strong solar proton eruption. The polar ionosphere was influenced directly by solar particle events, and thus affected the distribution and amplitude of the conductance in the ionosphere. For simplicity, we do not consider the

influence of the fine structure of the ionosphere, for we emphasize the large-scale structures and their variations of the magnetosphere. Due to the extreme solar wind conditions, the saturation level of the cross polar potential drop for this event (about 2000 kV) is much larger than the value for a typical magnetic storm (about 150–250 kV). The simulation shows that the reconnection voltage for the Carrington Event is 5 to 6 times higher than that for a normal storm, resulting in a large amount of solar wind energy to enter the inner magnetosphere and thus causing strong space weather phenomena. In the magnetotail, magnetic reconnection occurs in the central plasma sheet under the impact of the strong southward IMF B_Z. As shown in Figure 2(b), high-speed flows in opposite directions appear at $X = \sim -9$ R_E, where is the outflow region of a magnetic reconnection. The earthward high-speed flows carry large quantities of solar wind energy into the inner magnetosphere, and thereby affect the convection structure of inner magnetosphere and relevant electrodynamics in the magnetosphere-ionosphere coupling region, and further influence the ionosphere and geomagnetic activities.

3 Discussion and summary

When the Carrington Event occurred in 1859, humans were not as much dependent on the space-borne and ground-based high-technology systems as they are today. At present, the drastic changes of geospace environment caused by solar activities can affect aerospace, communication, navigation, positioning, and electric power system, etc. With the approaching of the 24th solar cycle peak year (2012–2014), the impacts of super solar storms on geospace environment have drawn more and more attentions. Super solar storms are low probability, but are high risk space disasters. Owing to the lack of events under superstorms, the relevant empirical formulas about geospace environment elements usually do not apply to such extreme conditions. In this work, we start with the geomagnetic observations of the Carrington Event in 1859, to estimate the interplanetary conditions at that time. Taking those parameters as input, we quantitatively analyze the responses of the earth's magnetosphere-ionosphere system to such an extreme intense solar storm by adopting the global 3D PPMLR-MHD model. The relevant values of geospace environment parameters like the magnetospheric large-scale structures, region-1 FAC, cross polar potential drop are summarized and listed in Table 1. For comparison, we calculate the parameters for the situations before and after the impact of the super storm. The main findings include: 1) the dayside magnetopause and bow shock are compressed to 4.3 and 6.0 R_E, and their flanks are also strongly compressed. The magnetopause shifts inside the geosynchronous orbit, exposing geosynchronous satellites in the solar wind in the magnetosheath; 2) during the storm, the region-1 FAC increases by about 60 times, and the cross polar potential drop increases by about 80 times; the reconnection voltage is about 5 to 6 times larger than the average storms. This means that a larger amount of the solar wind energy enters the magnetosphere, and results in strong space weather phenomena.

Table 1 Geospace environment elements before and after the superstorm

		Before	After
Position of magnetopause (R_E)	X_M	8.5	4.3
	Y_M	13.0	6.5
	Z_M	13.5	7.7
Position of the bow shock (R_E)	X_M	12.0	6.0
	Y_M	21.5	12.0
	Z_M	21.5	12.5
Region-1 FAC	Current density maximum ($\mu A/m^2$)	0.15	7.43
	Current amount (MA)	0.22	13.08
Cross polar potential drop (kV)		10.6	868.2

We thank academician Wei FengSi, Professor Hu YouQiu, and all the members of NSFC's space weather innovation research group for their guidances of this work. We also acknowledge the support of high performance computing provided by the Major National Science and Technology Infrastructure, the Meridian Project. This work was supported by National Natural Science Foundation of China (Grant Nos. 40921063, 40974106, 40831060), and the special fund for State Key Laboratory of Ministry of Science and Technology.

1 Cliver E W, Svalgaard L. The 1859 solar-terrestrial disturbance and the current limits of extreme space weather activity. Solar Phys, 2004, 224: 407–422
2 Clauer C R, Siscoe G. The great historical geomagnetic storm of 1859: A modern look. Adv Space Res, 2006, 38: 117–118
3 Green J L, Boardsen S. Duration and extent of the great auroral storm of 1859. Adv Space Res, 2006, 38: 130–135
4 Odenwald S, Green J, Taylor W. Forecasting the impact of an 1859-calibre superstorm on satellite resources. Adv Space Res, 2006, 38: 280–297
5 Shue J H, Chao J K, Fu H C, et al. A new functional form to study the solar wind control of magnetopause size and location. J Geophys Res, 1997, 102: 9497–9511
6 Lin R L, Zhang X X, Liu S Q, et al. A three-dimensional asymmetric magnetopause model. J Geophys Res, 2010, 115, doi: 10.1029/2009JA014235
7 Shue J H, Song P, Russell C T, et al. Magnetopause location under extreme solar wind conditions. J Geophys Res, 1998, 103: 17691–17700
8 Guo X C, Wang C, Hu Y Q, et al. Bow shock contributions to region 1 field- aligned current: A new result from global MHD simulations. Geophys Res Lett, 2008, 35: L03108, doi: 10.1029/2007GL032713
9 Ridley A J, De Zeeuw D L, Manchester W B, et al. The magnetospheric and ionospheric response to a very strong interplanetary shock and coronal mass ejection. Adv Space Res, 2006, 38: 263–272
10 Powell K, Roe P, Linde T, et al. A solution-adaptive upwind scheme for ideal magnetohydrodynamics. J Comput Phys, 1999, 154: 284–309
11 Tsurutani B T, Gonzalez W D, Lakhina G S. The extreme magnetic storm of September 1–2, 1859. J Geophys Res, 2003, doi: 10.1029/2002JA009504
12 Li X L, Temerin M, Tsurutani B T, et al. Modeling of 1–2 September 1859 super magnetic storm. Adv Space Res, 2006, 38: 273–279

13 Temerin M, Li X. A new model for the prediction of *Dst* on the basis of the solar wind. J Geophys Res, 2002, 107: 1472
14 Wang C, Li H, Richardson J D, et al. Interplanetary shock characteristics and associated geosynchronous magnetic field variations deduced from sudden impulses observed on the ground. J Geophys Res, 2010, 115, doi: 10.1029/2009JA014833
15 Hu Y Q, Guo X C, Wang C. On the ionospheric and reconnection potentials of the earth: Results from global MHD simulations. J Geophys Res, 2007, 112, doi: 10.1029/2006JA012145
16 Li H, Wang C, Kan J R. Mid-day magnetopause shifts earthward of geosynchronous orbit during geomagnetic superstorms with *Dst* < −300 nT. J Geophys Res, 2010, 115: A08230, doi: 10.1029/2009JA014612
17 Liou K, Wu C C, Lepping R P, et al. Midday sub-auroral patches (MSPs) associated with interplanetary shocks. Geophys Res Lett, 2002, 29: 16–20
18 Fedder J A, Lyon J G, Slinker S P, et al. Topological structure of the magnetotail as a function of interplanetary magnetic field direction. J Geophys Res, 1995, 100: 3613
19 Siscoe G L, Erickson G M, Sonnerup B U O, et al. Hill model of transpolar potential saturation: Comparisons with MHD simulations. J Geophys Res, 2002, 107, doi: 10.1029/2001JA000109
20 Hill T W, Dessler A J, Wolf R A. Mercury and Mars: The role of ionospheric conductivity in the acceleration of magnetospheric particles. Geophys Res Lett, 1976, 3: 429–432
21 Hill T W. Magnetic coupling between solar wind and magnetosphere: Regulated by ionospheric conductance? Eos Trans AGU, 1984, 65: 1047